

Experimental Extraction of Effective Refractive Index and Thermo-Optic Coefficients of Silicon-on-Insulator Waveguides Using Interferometers

Sarvagya Dwivedi, Alfonso Ruocco, Michael Vanslembrouck, Thijs Spuesens, Peter Bienstman, Pieter Dumon, Thomas Van Vaerenbergh, and Wim Bogaerts

Abstract—We propose and demonstrate an accurate method of measuring the effective refractive index and thermo-optic coefficient of silicon-on-insulator waveguides in the entire C-band using three Mach-Zehnder interferometers. The method allows for accurate extraction of the wavelength dispersion and takes into account fabrication variability. Wafer scale measurements are performed and the effective refractive index variations are presented for three different waveguide widths: 450, 600, and 800 nm, for the TE polarization. The presented method is generic and can be applied to other waveguide geometries and material systems and for different wavelengths and polarizations.

Index Terms—Effective refractive index, thermo-optic coefficients, waveguides, wavelength filtering devices.

I. INTRODUCTION

SILICON photonics is a rapidly growing field with applications from optical interconnects to bio-sensing. The silicon-on-insulator (SOI) platform has been a promising platform for mass scale production of silicon photonics devices since it can use complementary metal–oxide–semiconductor (CMOS) process technology for fabrication. This offers a scaling avenue to large-volume production at an affordable cost.

SOI can be used to define waveguides with a high refractive index contrast between core and cladding. This enables dense integrated photonic circuits with submicron waveguide cores and sharp bends. However, the high index contrast and small

waveguide dimensions can translate small variations in waveguide width and thickness into large fluctuations in the effective refractive index [1]. This is a potential weakness to this platform and extremely precise fabrication is required to achieve a good yield. Also, the high refractive index contrast makes the waveguide properties quite dispersive with wavelength.

In order to design effectively in such a waveguide platform, the exact value of the optical properties should be known, including their wavelength dependence and the statistics of their variability. Many optical properties, such as waveguide loss, can be collected from optical measurements on fabricated devices. But this is difficult for the *effective refractive index* (n_{eff}) of the waveguide.

The effective refractive index is a very critical parameter in the design of wavelength filters [2], [3]. It determines the exact condition of constructive interference, and therefore the central operating wavelength of a filter. Effective index changes can therefore cause a wavelength shift of a filter: in silicon wire waveguides this shift is approximately 1 nm for 1 nm of waveguide width change and around 1.4 nm for 1 nm change in waveguide thickness. Similar to geometry variations, local and environmental temperature fluctuations can cause a change in effective index: since silicon has a high thermo-optic (TO) coefficient of $1.86 \times 10^{-4} \text{ K}^{-1}$, this can result in a filter wavelength shift of 80 pm/K [4].

Given the extreme sensitivity of a silicon wire waveguide to the exact geometry, it is important to accurately characterize the effective index, including its dispersion, without perturbing the actual waveguide geometry. Existing methods to extract the dispersion such as prism coupling are either not suited for high refractive index waveguides, or actively perturb the waveguide [5]. Non-invasive methods such as ellipsometry cannot be easily applied to narrow waveguides. Techniques using scattering with weak higher-order periodic perturbations effectively perturb the waveguide, but also change the local pattern density, and thus could even influence the fabrication process [1].

Methods which rely on relative features in the transmission spectrum of interferometric devices will measure the group index n_g rather than the effective index n_{eff} [6]. Because silicon wire waveguides are very dispersive, n_g and n_{eff} are very different, and highly wavelength dependent. Knowing the group index, it is theoretically possible to integrate the effective index,

Manuscript received July 12, 2015; revised August 27, 2015; accepted August 28, 2015. Date of publication September 3, 2015; date of current version September 25, 2015.

S. Dwivedi, A. Ruocco, M. Vanslembrouck, T. Spuesens, and P. Bienstman are with the Photonics Research Group, Department of Information Technology, imec and Center for Nano- and Biophotonics, Ghent University, Ghent B-9000, Belgium (e-mail: sarvagya.dwivedi@intec.ugent.be; alfonso.ruocco@intec.ugent.be; Michael.Vanslembrouck@intec.ugent.be; Thijs.Spuesens@intec.ugent.be; peter.bienstman@ugent.be).

P. Dumon and W. Bogaerts are with the Photonics Research Group, Department of Information Technology, imec and Center for Nano- and Biophotonics, Ghent University, Ghent B-9000, Belgium and also with Lueda Photonics, Dendermonde 9200, Belgium (e-mail: pieter.dumon@intec.ugent.be; wim.bogaerts@ugent.be).

T. Van Vaerenbergh was with the Photonics Research Group, Department of Information Technology, imec and Center for Nano- and Biophotonics, Ghent University, Ghent B-9000, Belgium. He is now with Hewlett-Packard Labs., Palo Alto, CA 94304 USA (e-mail: Thomas.VanVaerenbergh@intec.ugent.be).

Color versions of one or more of the figures in this paper are available online at <http://ieeexplore.ieee.org>.

Digital Object Identifier 10.1109/JLT.2015.2476603

but this can result in an ambiguous solution. Therefore, a method is needed to extract the effective index (as well as the group index) unambiguously and including their wavelength dispersion and temperature dependence.

Simulation of a waveguide cross section to extract the waveguide mode properties is also possible, but at best it gives a good estimate of the effective index. In practice, the geometry of a buried silicon wire is hard to measure experimentally, even with high-resolution SEM. Also, boundary effects in the material properties can also affect the effective index but cannot be perceived by visual or SEM inspections. However, simulations can provide a first estimate which we also use in our method as a starting point to improve the accuracy.

We present a simple approach to accurately measure the n_{eff} of a silicon photonics wire. Our method uses three Mach-Zehnder interferometers (MZI) designed with the same photonic wire located as close as possible to each other. MZIs are good candidates as they are simple in design, linear in phase response and flexible in choosing the filter order. When using ring resonators, the measurements must be done at sufficiently low power levels to avoid nonlinear effects [7]–[9]. Also, the resulting measurement will be a weighted average of the bends, the straight sections and the coupling sections. The measurement is even more complicated because for the highest accuracy the ring needs to be critically coupled, requiring precise control of the waveguide to ring gap dimension.

In our method we use two MZIs with a low order m , i.e., a large *free spectral range* (FSR), which allow us to estimate the order of the filter correctly within the C-band. The third MZI has a much higher order and a small FSR, which helps us to extract the wavelength dependence of the group index (n_g). To extract the TO coefficients, we measure the same MZIs at different temperatures and then extract the wavelength sensitivity of the spectrum with respect to temperature. We also perform and present wafer-scale measurements for three different waveguide widths of 450, 600 and 800 nm, respectively. Our method is generic in nature and should work for all integrated waveguide platforms. We already reported preliminary results of this method [10]. In this paper the method is fully elaborated and demonstrated for different waveguide sections, including wafer-scale statistics and TO coefficients extraction.

II. METHOD

The effective refractive index of an SOI waveguide at a given wavelength is a function of the materials, the waveguide cross-sectional geometry and environmental temperature. We can conceptually simplify this as follows.

A. Effective Index Model

$$n_{\text{eff}}(\lambda) = f(w, h, T) \quad (1)$$

where w , h is waveguide width and thickness, respectively, and T is the environment temperature.

The eigenmode simulations for the initial estimate of the SOI waveguide mode are performed by the finite element method

from COMSOL, taking a wavelength and temperature dependent material model. The wavelength and temperature dependent refractive index material model of silicon and oxide at room temperature is given by the Sellmeier equation [11]–[13]:

$$n_{\lambda, T}^2 - 1 = \sum_{i=1}^3 \frac{S_i(T)\lambda^2}{\lambda^2 - \lambda_i^2(T)} \quad (2)$$

where $S_i(T)$ is a temperature dependent Sellmeier coefficients. At $\lambda = 1550$ nm and room temperature, the value of n_{Si} is 3.4777 and for n_{SiO_2} is 1.4440. The TO coefficient ($\frac{dn}{dT}$) at 1550 nm is $1.86 \times 10^{-4} K^{-1}$ for silicon and $1.0 \times 10^{-5} K^{-1}$ for oxide, here T is the temperature in Kelvin (K).

B. Extracting the Effective Index From a Single MZI

In any given wavelength filter, as in our MZI, we get constructive interference at the output when

$$m.\lambda_{\text{res}} = n_{\text{eff}}(\lambda_{\text{res}}).\Delta L \quad (3)$$

where λ_{res} is resonance wavelength, m is the filter order, $n_{\text{eff}}(\lambda_{\text{res}})$ is effective index of the waveguide at that wavelength and ΔL is the physical path length difference.

From Eq. (3), if we know the resonance wavelength and the filter order, we can extract the effective index at that wavelength. In normal practice, we designed the filter with a known order m , using a prior estimate of n_{eff} . However, if the possible deviations in n_{eff} from our design estimate become too large, we cannot be sure about the order. Identifying the order of a filter response is essential, as this gives us an absolute reference for the calculation of the effective index. For a given design order m , the largest change Δn_{eff} that we can allow to successfully identify the same order m of the fabricated design is

$$\Delta n_{\text{eff}} = \frac{2}{2m+1}. \quad (4)$$

We can assume that in first order, Δn_{eff} is due to a change in width Δw and height Δh :

$$\Delta n_{\text{eff}} = \frac{dn_{\text{eff}}}{dw} \cdot \Delta w + \frac{dn_{\text{eff}}}{dh} \cdot \Delta h. \quad (5)$$

Here, dn_{eff}/dw and dn_{eff}/dh is the change in n_{eff} due to waveguide width and thickness, respectively, at a given temperature. These trends we can quite reliably extract from simulations. The maximum allowed Δn_{eff} for a wavelength filter of a given order is shown in Fig. 1. We see that for higher-order filters, it becomes difficult to estimate the interference order unless the fabrication process is very precise.

Fig. 1 also shows the maximum Δn_{eff} for three different waveguides widths, i.e., 450, 600 and 800 nm for a fabrication process with an accuracy of ± 20 nm for waveguide linewidth and ± 5 nm for waveguide thickness which is estimated from Eq. (5) [1]. As can be expected, the wider waveguides will suffer less from small absolute linewidth variations than the narrow waveguide. For the 450 nm wide waveguide the field strength of the fundamental TE mode is much stronger on the side wall boundaries than width the 600 and 800 nm waveguides. The specified variation of ± 5 nm on the waveguide thickness

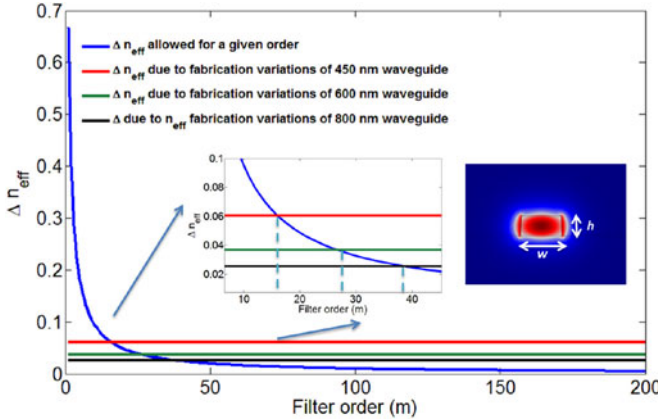


Fig. 1. The estimated Δn_{eff} allowed and maximum fabrication variations for three different waveguides 450, 600 and 800 nm for increasing filter order m . Inset 1: Zoomed plot showing the region of operation of which order to choose when there maximum fabrication in a different waveguides. Inset 2: Simulated 2-D TE mode profile of 450 nm wide and 215 nm SOI waveguide with oxide as top cladding at room temperature.

does not affect the TE mode as much, but it will have a much stronger impact on the TM mode. For this work we focus on the fundamental TE mode but the method can be extended to the TM mode.

The intersection of the three horizontal traces with the blue trace gives us the maximum order of a wavelength filter where we can still identify the order m with confidence. For 450, 600 and 800 nm, the values of m are 17, 27 and 38 respectively. When designing a filter to use for refractive index extraction, we should pick an order below these values.

When we design our filter with a sufficiently low order, the possible changes in the refractive index will be low enough such that

$$n_{\text{eff}}^{(m-1)} + \Delta n_{\text{eff}} < n_{\text{eff}}^{(m)} - \Delta n_{\text{eff}} \quad (6)$$

$$n_{\text{eff}}^{(m)} + \Delta n_{\text{eff}} < n_{\text{eff}}^{(m+1)} - \Delta n_{\text{eff}}. \quad (7)$$

This means that we can unambiguously associate each λ_{res} of constructive interference with an order m . This is shown in Fig. 2, where we simulated an MZI with 450 nm wide waveguide case for $m = 15$ (middle curve). The error bars indicate our initial uncertainty on the n_{eff} . The top and bottom curve then show the extracted index if we would have made an error of ± 1 in the order m . It is clear that the curves do not overlap, even when taking into account the uncertainty. This means that we can confidently use a filter with this order for the waveguides in this fabrication process.

C. Using High-Order MZI

A low-order MZI allows us to accurately identify the order of interference at λ_{res} and thus the effective index at that wavelength. However, in the typical wavelength range of the C-band around 1550 nm, this will result in at most two peaks and valleys in the transmission spectrum. This makes it difficult to extract an accurate model for the wavelength dispersion.

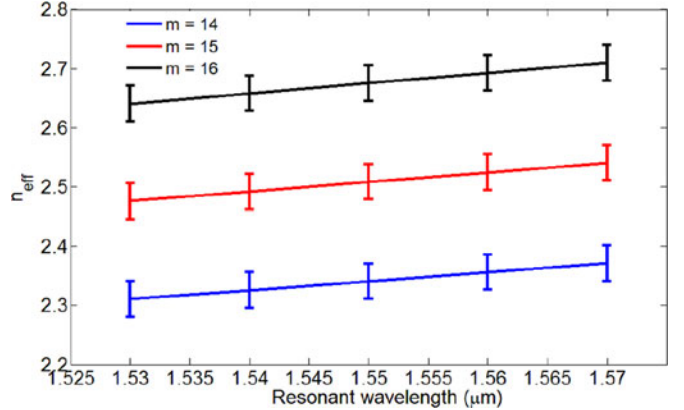


Fig. 2. Simulated effective index for neighboring order at resonant wavelengths for 450 nm waveguide. Shown error margin is due to the maximum fabrication variations.

To compensate for this, we introduce another MZI with a much higher interference order M . From this we can get a large number of peaks and valleys in the wavelength band. The FSR of the filter is the difference between two consecutive peaks of the filter:

$$\text{FSR} = \lambda^2 / n_g \cdot \Delta L. \quad (8)$$

From this device, extraction of $n_g(\lambda)$ of the waveguide is possible by extracting the wavelength dependent FSR from the transmission measurements. With above these information we can extract the coefficients of modified Taylor expansion in $n_{\text{eff}}(\lambda)$ and $n_g(\lambda)$, based on the reference of the known $n_{\text{eff}}(\lambda_0)$ and is given by:

$$n_{\text{eff}}(\lambda) = a + b\Delta\lambda + c(\Delta\lambda)^2 \quad (9)$$

$$n_g(\lambda) = a - b\lambda_0 - c(\lambda_0 \cdot \Delta\lambda) \quad (10)$$

where $a = n_{\text{eff}}(\lambda_0)$, $b = \frac{dn_{\text{eff}}}{d\lambda}$ and $c = \frac{d^2 n_{\text{eff}}}{d\lambda^2}$. For the TE waveguide, we can ignore the further terms of the Taylor expansion, since they are comparable to the fitting error for the designed TE-polarized waveguide. For TM waveguides, the higher-order terms would be non-negligible. From low order MZI, a can be extracted without an error. The b and c coefficients are extracted by accurately by higher order filter. Combining these two we have all the coefficients and accurate extraction of $n_{\text{eff}}(\lambda)$ and $n_g(\lambda)$.

D. A Second Low-Order MZI

Because we use two different devices for extracting a single effective index, there is always the possibility that local variability between the two devices introduces errors in our extraction procedure. To reduce this error, we introduce a second low-order MZI, with an order $m' > m$, but still lower than the maximum allowed order needed to identify it unambiguously. We design this second MZI to have the same resonance wavelength as the original MZI:

$$\frac{\Delta L}{m} = \frac{\Delta L'}{m'}. \quad (11)$$

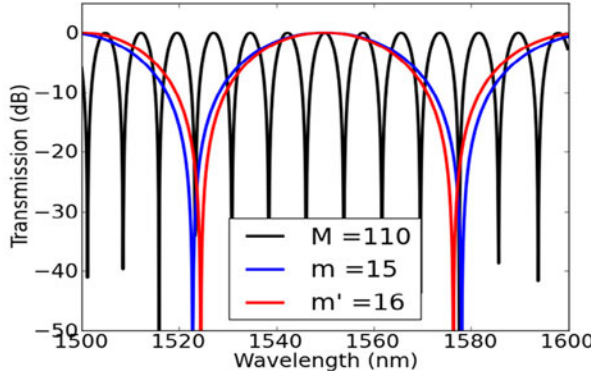


Fig. 3. Simulated circuit transmission of an MZI filter made out of 450 nm wide and 215 nm thick SOI waveguide with $m = 15$, $m' = 16$ and $M = 110$, respectively.

We can now estimate the local variations of the effective index Δn_{eff} from the shifts of the two resonances λ_{res} and λ'_{res} , which ideally should be zero

$$\Delta n_{\text{eff}} = 2 \cdot \frac{m' \cdot \lambda'_{\text{res}} \cdot \Delta L - m \cdot \lambda_{\text{res}} \cdot \Delta L'}{m' \cdot \lambda'_{\text{res}} \cdot \Delta L + m \cdot \lambda_{\text{res}} \cdot \Delta L'}. \quad (12)$$

For our experiments, we chose two MZIs with low order $m = 15$ and $m' = 16$, to satisfy the condition on fabrication variations mentioned in Eq. (4)–(7) and $M = 110$ to get the $n_g(\lambda)$ in the wavelength of interest. For this, we used a simulated model of n_{eff} , calculated using a finite-element fully vectorial mode solver, and using a geometry extracted from a cross-sectional SEM (XSEM) image. With this parameters, even with a significant deviation from the model, we are able to still identify the peaks of the right order.

E. Extraction of TO Coefficient

For extraction of the TO coefficient of a waveguide, the wavelength sensitivity with respect to temperature needs to be measured and it is given by [4] :

$$\frac{dn}{dT}|_{\lambda_{\text{res}}} = \frac{n_g}{\lambda_{\text{res}}} \frac{d\lambda}{dT}. \quad (13)$$

The TO coefficient of the waveguide is extracted after first extracting the waveguide group index n_g at a given wavelength λ_m and filter transmission at different temperatures T .

An alternative method to extract the TO coefficient is to extract $n_{\text{eff}}(\lambda_{\text{res}})$ from the low order MZIs for different temperatures and then use Eq. (3) directly at a given wavelength.

III. DESIGN AND FABRICATION

The MZIs are simulated and designed for three different waveguides, i.e., 450, 600 and 800 nm wide respectively and with 215 nm thick silicon wires for values $m = 15$, $m' = 16$ and $M = 110$, respectively. The full eigenmode solutions as discussed in Section II are fed to the circuit solver CAPHE to get the transmission response at fixed room temperature [14], [15]. The simulated transmission of the three 450 nm MZI filters for $m = 15$, $m' = 16$ and $M = 110$ is shown in Fig. 3. As

they have been designed for that condition, the three simulations show constructive interference at λ_{res} of 1550 nm.

Devices are designed using the IPKISS by Lueda Photonics design framework, which generates the layouts directly from a parametric description of the MZI [15].

Because the quality of the transmission trace is essential for an accurate extraction, we have designed the test circuits to minimize reflections. There are different contributions of reflection in SOI based wavelength devices. The major contributions to reflection are from the grating couplers to and from the chip. Therefore, we use compact off-axis grating couplers with reduced back reflections [16]. They are designed at an angle of 45° to the in-plane fiber axis, and they direct backreflections away from the input waveguide. This reduces back-reflection from -20 to -50 dB.

The arms of the MZI are designed with a relatively large bend radius of $20 \mu\text{m}$ to avoid reflections from the straight-bend interface and to minimize the loss. The arms are symmetric except for the vertical straight section which incorporates the actual delay ΔL . This cancels out possible effects of bend-radius dependence of n_{eff} .

Our device focuses on measuring and extracting the n_{eff} of straight photonic wires. It can be extended to extract the bend mode waveguide refractive index by incorporating the delay line in the bend sections.

The side wall roughness of the waveguide is unavoidable and depends upon the fabrication. This effect is prominent in 450 nm wide waveguides and gradually decreases for wider waveguides, i.e., for 600 and 800 nm.

For equal splitting and combining the light, the device uses wide band 1×2 multimode interference (MMI). By using a symmetric splitter and combiner we reduce the effect of wavelength dependence in directional couplers, and the couplers do not inherently introduce a phase delay between the arms.

The fabrication of our device has been done in the imec 200 mm CMOS pilot line using SOI wafers with an nominal 220 nm of silicon and $2 \mu\text{m}$ of buried oxide and $1.25 \mu\text{m}$ of top oxide [17]. During the processing, approximately 5 nm of silicon is removed.

Camera images of all three MZIs designed with 600 nm wide waveguide and SEM image of one of the fabricated MZI with $M = 110$ are shown in Fig. 4.

IV. MEASUREMENTS AND ANALYSIS

A. Device Measurements

The transmission measurements are performed in a thermally controlled environment to eliminate the effect of the high TO coefficient of silicon, which can induce a wavelength peak shift about of 80 pm/K. The device transmission is first normalized to that of a simple straight waveguide to eliminate the grating coupler spectrum. The 10 dB bandwidth of the grating coupler is around 80 nm from 1505 to 1585 nm. The on-chip insertion loss of the MZI is less than 0.3 dB.

The normalized transmission spectrum is fitted using nonlinear least square method and cosine square interferometric model given by Eq. (9) and (10) as a base function. The fitting

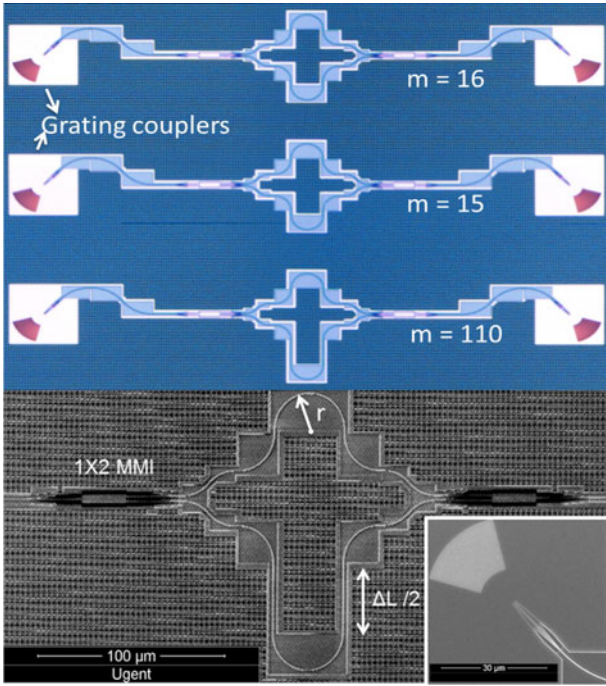


Fig. 4. (a) Camera image of set of fabricated devices for 600 nm wide waveguide and (b) SEM image of fabricated MZI with $M = 110$ showing the MMI, bend radius r and path length difference ΔL . Inset: Low reflection compact grating coupler.

procedure minimizes the RMS error between the measured and theoretical transmission trace. For a proper statistical analysis of these errors we use a re-sampling technique. The RMS of the fitting error is used as the standard deviation of a random Gaussian noise model of the measurement perturbation. This procedure is reiterated 1000 times to obtain a statistical relevant dataset. The results of these fittings are used to define the standard deviations of the a , b and c coefficients used in Eq. (9) and (10) to define $n_{\text{eff}}(\lambda)$ and $n_g(\lambda)$.

The measured and fitted the transmission spectra of the 3 MZIs designed for 450 nm are shown in Fig. 5. However, the measured width and thickness of the waveguide are closer to 470 ± 4 and 211 ± 2 nm, respectively, as extracted from SEM inspection. The other two waveguides, designed at 600 and 800 nm, are closer to the designed width, as shown in the SEM images.

The XSEM of the waveguide, the simulated mode profile of all the three waveguides, i.e., 470, 604 and 805 nm are shown in Fig. 6.

The extracted n_{eff} and n_g for all three waveguides over the entire C-band is shown in Fig. 7.

The extracted n_g from the higher order filter and then the n_{eff} from the low order filter of the different waveguide widths at 1550 nm is shown in Table I.

As shown in Table I the (\pm) contribution in the n_{eff} and n_g extraction comes from the measurement error and the standard deviation (σ) is from the fitting.

The mismatch between the extracted value and the simulations of the waveguide according to XSEM (with best fitted width, taking into account the uncertainty of the SEM measure-

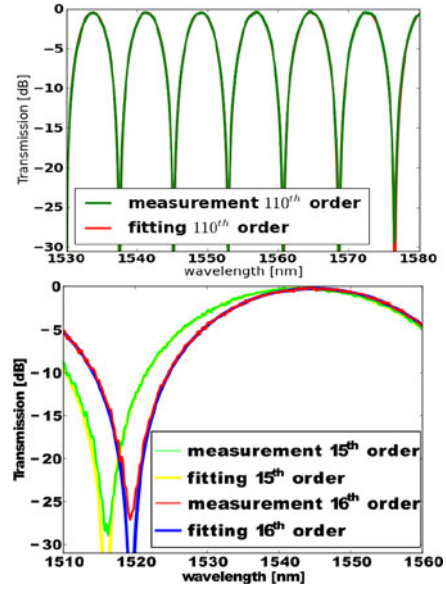


Fig. 5. Measured and fitted normalized spectrum of MZI designed with 450 nm wide and 215 nm thick silicon waveguide (a) higher filter order and (b) lower filter order.

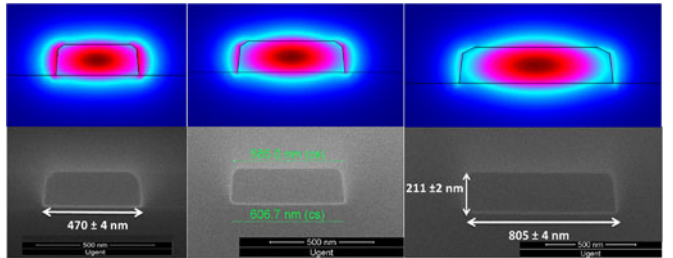


Fig. 6. Simulated mode profile and XSEM image of 470, 604 and 805 nm wide and 211 nm thick waveguides. Side wall angles of the trapezoidal waveguides can be easily seen in the SEM. Silicon corner rounding in the waveguide is due to the passive short loop specific process; which involves oxide deposition after the hardmask removal.

ment itself) mainly comes from local environmental variations, and fabricated waveguide geometrical non-idealities.

The local variability can be estimated by extracting the n_{eff} from $m' = 16$ as well and compare with $m = 15$. The variation of Δn_{eff} for 470 nm wide wire due to this is around ± 0.0015 .

B. TO Coefficient Measurements

For the measurements of the TO coefficient ($\frac{dn}{dT}$) we placed the fabricated chip on a thermally controlled chuck with a resistive heater and temperature sensor. The MZIs transmission is characterized at different temperatures. The spectrum gets red shifted with increase in temperature. The shifted spectrum is fitted in the similar way as explained in previous section and by Eq. (13) the TO coefficient of the waveguides can be extracted. The extracted TO coefficients for all the three waveguides are shown in Fig. 8.

The error contribution in TO coefficient extraction can be mainly attributed to small thermal fluctuations in the chuck.

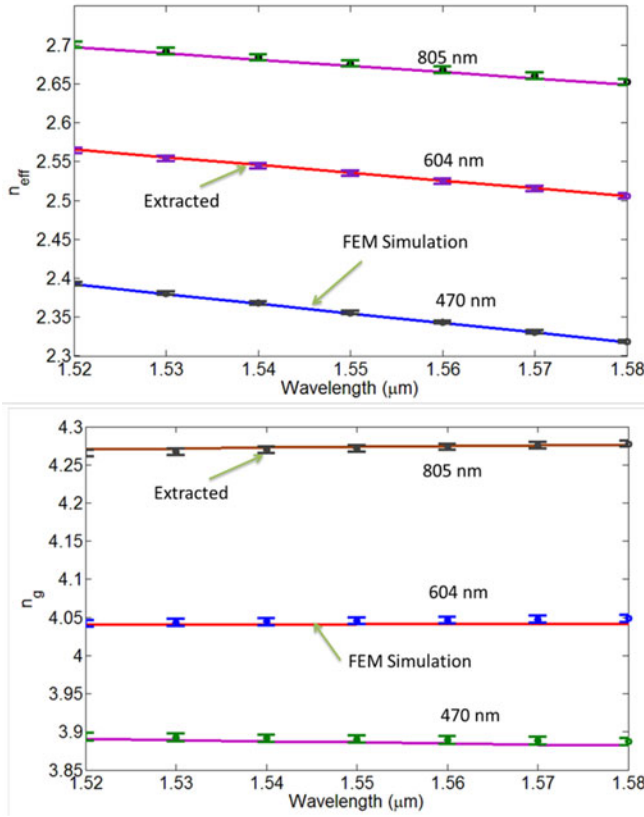


Fig. 7. (a) Simulated and extracted n_{eff} of 470, 604 and 805 nm wide waveguides and (b) simulated and extracted n_g over the C-band.

TABLE I
TABLE SHOWING THE EXTRACTED n_{eff} AND n_g

Waveguide	n_{eff}	n_{eff} fitting σ	n_g	n_g fitting σ
470 nm	2.355 ± 0.002	1.8007e-6	4.2739 ± 0.0042	3.963e-5
604 nm	2.534 ± 0.0035	3.806e-6	4.0453 ± 0.0045	4.127e-5
805 nm	2.67 ± 0.004	7.7095e-6	3.8902 ± 0.005	4.321e-5

C. Wafer Scale Measurements

We characterized these devices over an entire wafer using a fully automatic optical probe station. The wafer map and distribution plot of extracted n_{eff} and n_g for 470, 600 and 800 nm wide and 211 nm thick waveguides at 1550 nm are shown in Figs. 9–11, respectively. Across the wafer, for 470 nm waveguide at 1550 nm, the mean value and standard deviation of n_{eff} is 2.360 and 0.008 and for n_g is 4.287 and 0.018, respectively. For the 600 nm waveguide the mean value and standard deviation of n_{eff} is 2.533 and 0.006 and for n_g is 4.045 and 0.02. And, for the 800 nm wide waveguide, the mean value and standard deviation of n_{eff} is 2.679 and 0.008 and for n_g is 3.924 and 0.01. The line width was measured using top-down SEM (TDSEM) provided by foundry at three different locations of the wafer maps. The deviation of the extracted

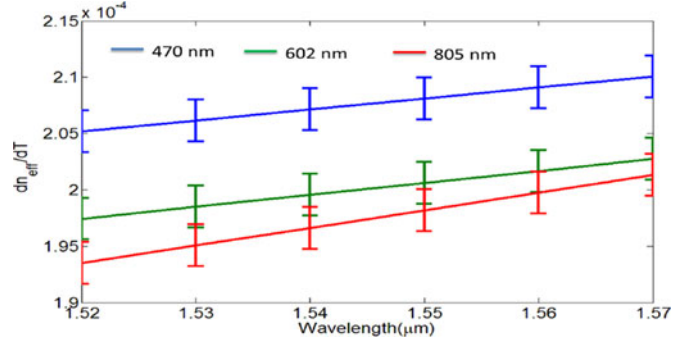


Fig. 8. Extracted dn_{eff}/dT of 470, 602 and 805 nm wide waveguides.

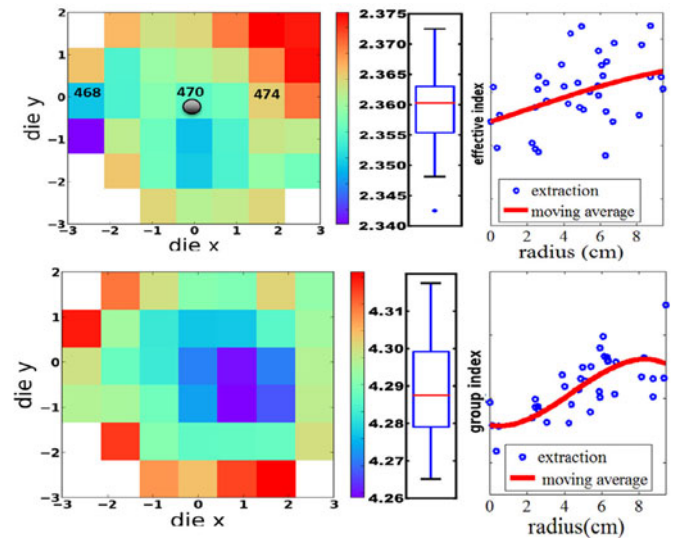


Fig. 9. Wafer map, distribution and radial plot of 470 nm wide fabricated waveguide at 1550 nm. Thickness variation is 211 ± 2 nm and σ of linewidth variation is 5 nm. TDSEM in nanometer at three locations. (a) n_{eff} and (b) n_g .

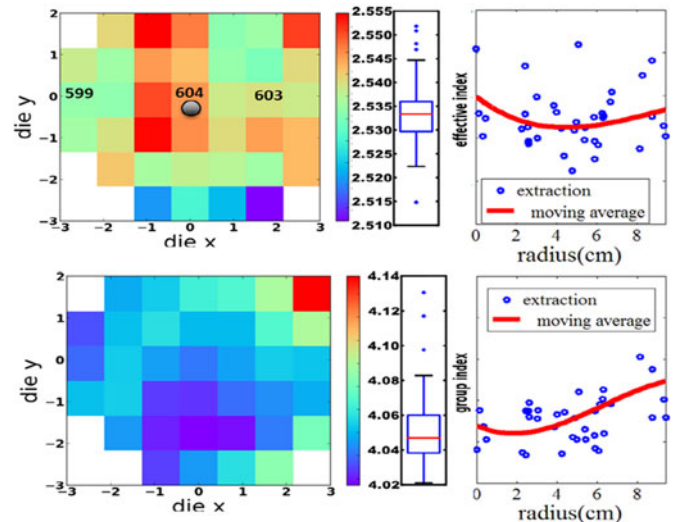


Fig. 10. Wafer map, distribution and radial plot of 604 nm wide fabricated waveguide at 1550 nm. Thickness variation is 211 ± 2 nm and σ of line width variation is 4 nm. TDSEM in nanometer at 3 locations. (a) n_{eff} and (b) n_g .

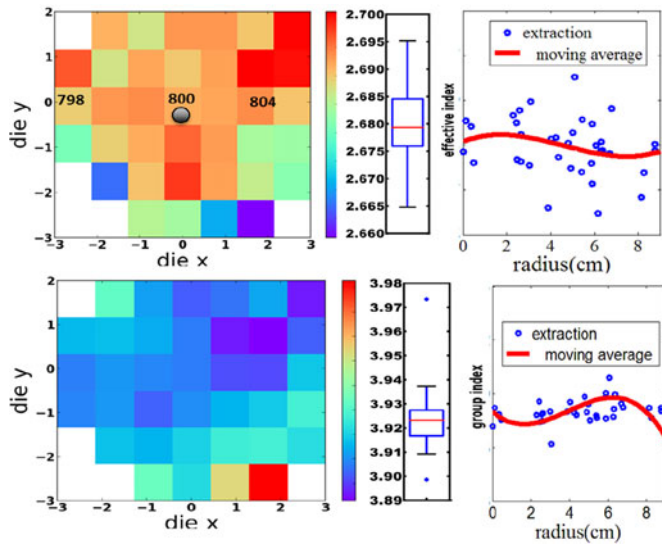


Fig. 11. Wafer map, distribution and radial plot of 805 nm wide fabricated waveguide at 1550 nm. Measured thickness is 211 ± 2 nm and σ of line width variation is 4 nm. TDSEM in nanometer at three locations. (a) n_{eff} and (b) n_g .

effective and group indices is mainly influenced by two effects: the thickness and line width variation over the wafer. Thickness variation is due to the SOI polishing and can be considered to be slow process across the wafer. As provided by the foundry it is only a few nanometer over the entire wafer. The line width is correlated to lithographic process and it is performed using die based stepping which introduces discrete variations. The effect of the line width is therefore more pronounced than the effect of the thickness. As a result, we see a slow variation which is superimposed with a faster variation on the wafer maps.

V. CONCLUSION

We proposed and demonstrated a generic method for measuring the refractive index of dispersive SOI waveguides. By combining three MZIs of low and high order we can extract the wavelength and temperature dependent effective index and the group index unambiguously, and also obtain an estimate for the local variability of the effective index. It does not perturb the waveguide of local pattern density, which is essential in a high-contrast waveguide platform such as silicon photonics. This method can be applied to the TM polarization also and can be extended to other waveguide platforms as well.

ACKNOWLEDGMENT

The authors would like to thank Y. Li and B. Schneider for their useful discussions, L. Van Landschoot for SEM images and imec 200 mm p-line for device fabrication. They also want to thank P. Absil, A. Khanna, P. De Heyn, and J. Van Campenhout from imec for wafer data and processing details.

REFERENCES

- [1] S. Selvaraja, W. Bogaerts, P. Dumon, D. Van Thourhout, and R. Baets, "Subnanometer linewidth uniformity in silicon nanophotonic waveguide devices using CMOS fabrication technology," *IEEE J. Sel. Topics Quantum Electron.*, vol. 16, no. 1, pp. 316–324, Jan. 2010.
- [2] W. Bogaerts, S. K. Selvaraja, P. Dumon, J. Brouckaert, K. De Vos, D. Van Thourhout, and R. Baets, "Silicon-on-insulator spectral filters fabricated with CMOS technology," *IEEE J. Sel. Topics Quantum Electron.*, vol. 16, no. 1, pp. 33–44, Jan. 2010.
- [3] W. Bogaerts, S. Pathak, A. Ruocco, and S. Dwivedi, "Silicon photonics non-resonant wavelength filters: Comparison between AWGs, echelle gratings, and cascaded Mach-Zehnder filters," *Proc. SPIE*, vol. 9365, pp. 93 650H-1–93 650H-12, 2015.
- [4] S. Dwivedi, H. Dheer, and W. Bogaerts, "Maximizing fabrication and thermal tolerances of all-silicon fir wavelength filters," *IEEE Photon. Technol. Lett.*, vol. 27, no. 8, pp. 871–874, Apr. 2015.
- [5] J. Jägerská *et al.*, "Dispersion properties of silicon nanophotonic waveguides investigated with Fourier optics," *Opt. Lett.*, vol. 32, no. 18, pp. 2723–2725, Sep. 2007.
- [6] E. Dulkeith *et al.*, "Group index and group velocity dispersion in silicon-on-insulator photonic wires," *Opt. Exp.*, vol. 14, no. 9, pp. 3853–3863, May 2006.
- [7] X. Chen *et al.*, "Parameter extraction from fabricated silicon photonic devices," *Appl. Opt.*, vol. 53, no. 7, pp. 1396–1405, Mar. 2014.
- [8] A. Arbabi *et al.*, "Measurements of the refractive indices and thermo-optic coefficients of Si3N4 and SiOx using microring resonances," *Opt. Lett.*, vol. 38, no. 19, pp. 3878–3881, Oct. 2013.
- [9] W. Bogaerts *et al.*, "Silicon microring resonators," *Laser Photon. Rev.*, vol. 6, no. 1, pp. 47–73, 2012.
- [10] S. Dwivedi *et al.*, "Measurements of effective refractive index of SOI waveguides using interferometers," presented at the Advance Photonics OSA Technical Digest, Boston, MA, USA, 2015, Paper IM2A.6.
- [11] B. Tatian, "Fitting refractive-index data with the Sellmeier dispersion formula," *Appl. Opt.*, vol. 23, no. 24, pp. 4477–4485, Dec. 1984.
- [12] G. Ghosh, M. Endo, and T. Iwasaki, "Temperature-dependent Sellmeier coefficients and chromatic dispersions for some optical fiber glasses," *J. Lightw. Technol.*, vol. 12, no. 8, pp. 1338–1342, Aug. 1994.
- [13] B. J. Frey *et al.*, (2006). Temperature-dependent refractive index of silicon and germanium. [Online]. pp. 62 732J-1–62 732J-10. Available: <http://dx.doi.org/10.1117/12.672850>
- [14] M. Fiers *et al.*, "Time-domain and frequency-domain modeling of nonlinear optical components at the circuit-level using a node-based approach," *J. Opt. Soc. Am. B*, vol. 29, no. 5, pp. 896–900, May 2012.
- [15] [Online]. Available: <http://www.lucedaphotonics.com/>
- [16] Y. Li *et al.*, "Compact grating couplers on silicon-on-insulator with reduced backreflection," *Opt. Lett.*, vol. 37, no. 21, pp. 4356–4358, Nov. 2012.
- [17] P. P. Absil *et al.*, "Silicon photonics integrated circuits: A manufacturing platform for high density, low power optical I/O's," *Opt. Exp.*, vol. 23, no. 7, pp. 9369–9378, Apr. 2015.

Authors' photographs and biographies not available at the time of publication.